Available online at www.sciencedirect.com

ScienceDirect

www.elsevier.com/locate/jes

JES JOURNAL OF ENVIRONMENTAL SCIENCES

www.jesc.ac.cn

Kinetics and capacities of non-reactive phosphorus (NRP) sorption to crushed autoclaved aerated concrete (CAAC)

Shuting Shen[1,2], *Xiang Li*[1,2], *Zhuofan Geng*[1,2], *Xiwu Lu*[1,2,*]

[1] *School Energy and Environment, Southeast University, Nanjing 210096, China*
[2] *ERC Taihu Lake Water Environment Wuxi, Wuxi 214135, China*

ARTICLE INFO

Article history:
Received 20 May 2022
Revised 5 July 2022
Accepted 5 July 2022
Available online 15 July 2022

Keywords:
Non-reactive phosphorus
Crushed autoclaved aerated concrete
Phosphorus removal
Sorption
Wastewater treatment

ABSTRACT

With growing interest in resource recovery and/or reuse, waste materials have been considered a promising alternative for phosphorus (P) adsorption because they are low-cost and easily accessible. Crushed autoclaved aerated concrete (CAAC), as representative construction waste, has been extensively studied for P removal in ecological technologies such as treatment wetlands. However, most of the previous studies focused on the adsorption of orthophosphate, namely reactive phosphorus, and lacked attention to non-reactive phosphorus (NRP) which is widely present in sewage. This study presents the first investigation on the potential and mechanism of CAAC removing four model NRP compounds. Adsorption isotherm and kinetics of NRP onto CAAC indicate that the removal of NRP was a chemisorption process and also involved a two-step pore diffusion process. The desorption experiment shows that different NRP species showed varying degrees of desorption. Most NRP was irreversibly adsorbed on CAAC. Among the model compounds considered in this study, the adsorption capacity and hydrolysis rate of organophosphorus were much less than that of inorganic phosphorus. Moreover, the adsorption of different NRP species by CAAC in the mesocosm study was different from the results of laboratory adsorption experiments, and the possible biodegradation was essential for the conversion and removal of NRP. The findings confirmed the validity of CAAC for NRP removal and the potential advantages of CAAC in terms of costs and environmental impact. This study will contribute to a better understanding of NRP conversion and environmental fate and that can be the basis for a refined risk assessment.

Introduction

The utilization of mined phosphate rock is the basis of modern agriculture. Approximately 21 million tons of phosphate rock are mined annually for human use through the production of fertilizers and other industrial products, and almost 35% (6.3 ± 3 million metric tonnes/year) of the phosphorus (P) is lost into freshwater and coastal waters (Cordell and White, 2014). Human activities have made P enter the hydrosphere at rates over three times natural flow, leading to eutrophication (Smil, 2002), with adverse consequences for aquatic ecosystems, water quality, and recreation. More than 400 dead zones are known worldwide as a result of eutrophication, and the number is expanding at 10% per decade

* Corresponding author.
E-mail: xiwulu@seu.edu.cn (X. Lu).

https://doi.org/10.1016/j.jes.2022.07.006
1001-0742/

(Diaz and Rosenberg, 2008). The economic damages caused by eutrophication in the United States alone are estimated at US$2.2 billion annually (Dodds et al., 2009).

Total phosphorus (TP) is usually divided into reactive phosphorus (RP) and non-reactive phosphorus (NRP) based on colorimetric P detection methods to distinguish their bioavailability and the feasibility of processes for removing or recovering P (Gray et al., 2020). NRP contains acid-hydrolysable phosphorus (AHP) and organic phosphorus (OP) species which is not readily reactive and is largely classified as a non-bioavailable component (Rittmann et al., 2011). About 10% of TP in raw wastewater and up to 30–60% of TP in environmental water have been reported to consist of NRP (Venkiteshwaran et al., 2018). Although the relative fractions of NRP are widely variable, NRP can be one of the main P fractions and is widely present in many aquatic ecosystems (Lei et al., 2020). Further, NRP could be converted to RP when subjected to enzymatic degradation or photochemical conversion, which may significantly enhance the bioavailability of NRP to plants, microorganisms, and algae, thereby increasing the risk of eutrophication in water bodies (Rott et al., 2018). Therefore, NRP is an underestimated issue to limit eutrophication risks and establish a P cycle.

The types of NRP in water depend on the water source (water matrix, specific waterbody, and location/time). AHP mainly includes inorganic and organic polyphosphates, which can occur naturally and serve as energy reserves for microorganisms, and be also commonly used in fertilizers, preservatives, and detergents (Venkiteshwaran et al., 2018). Natural OP usually derived from plant or animal tissues, nucleic acids, nucleotides, and phospholipids in aquatic organisms. For example, adenosine monophosphate (AMP) is the natural OP containing phosphoester bond (P–O–C), which is bioavailable and ubiquitous in biological cells (Baldwin, 2013). Synthetic OP is commonly used in pesticides, herbicides, flame retardants, and plasticizers, and the P usually exists in the form of a direct P–X bond, where X is the electronegative group, such as C, S, N, or F. Unlike the phosphoanhydride bond (P–O–P) in polyphosphates and phosphoester bond (P–O–C), the phosphonates are characterized by the presence of a stable covalent carbon to phosphorus bond (C–P) (Huang and Zhang, 2011). In terms of global consumption, 2-phosphonobutane-1,2,4-tricarboxylic acid (PBTC), 1-hydroxyethane-1,1-diphosphonic acid (HEDP), ethylenediamine tetra (EDTMP) and diethylenetriamine penta (DTPMP) are important representatives of phosphonates (Rott et al., 2018). Unfortunately, due to the difficulty of analysis and lack of understanding of NRP composition and structure, very little is known about their concentrations and behavior in the environment. More efforts are needed to address the NRP-related research gaps.

Currently, numerous studies have been dedicated to P removal from waters, and orthophosphate can be relatively easily removed by enhanced biological P removal, precipitation, or adsorption (Rittmann et al., 2011). Adsorption has been proved to be an effective method to remove P from waters. Especially for phosphonates that are poorly biodegradable and exhibit excellent water solubility, adsorption is a more important route of elimination from the water phase (Knepper, 2003). However, the economy and sustainability of adsorbents have always been the main reasons limiting their application (Shen et al., 2020). With the popularization of the circular economy concept and the increasing awareness of the sustainable use of solid wastes, there is great interest in developing solid waste-based adsorbents for the purification of P-containing waters. Among them, construction wastes, such as bricks (Dires et al., 2019) and concrete blocks (Yang et al., 2012), have been considered as a promising adsorbent for P removal because it is efficient, economical, and environment friendly (Shi et al., 2017). P species and physicochemical characteristics are closely related to the adsorption and desorption of P, and also determine the P mobility and bioavailability (Pramanik et al., 2020). However, the previous studies have usually focused on the adsorption or desorption characteristics of orthophosphate while studies on P removal and recovery from NRP are rarely reported. As a result, NRP limits the final P removal efficiency and ultra-low leave P emissions.

In this study, four common model compounds (STPP, EDTMP, PBTC, and AMP) were individually tested to evaluate the ability of construction waste, namely crushed autoclaved aerated concrete (CAAC), to remove NRP species. The model compounds were chosen based on their structures and ubiquity in water columns. The adsorption isotherms and kinetic models were applied to discuss the adsorption behavior and mechanism of NRP on CAAC. Desorption experiments were conducted to determine the desorption capacity of different P species, thus evaluating the potential eutrophication risk and the bioavailability of adsorbed P. A batch-loaded mesocosm experiment was performed to evaluate the NRP removal performance of reactors filled with CAAC. This study provides an assessment of the reuse of construction wastes and NRP removal efficacy. The results of this study will contribute to a better understanding of NRP conversion and environmental fate and that can be the basis for a refined risk assessment.

1. Material and methods

1.1. *Materials*

Four model NRP compounds were selected in the study: sodium tripolyphosphate ($Na_5P_3O_{10}$, STPP), ethylenediamine tetra methylenephosphonic acid ($C_6H_{20}N_2O_{12}P_4$, EDTMP), 2-phosphonobutane-1,2,4-tricarboxylic acid ($C_7H_{11}O_9P$, PBTC) and adenosine 5'-monophosphate ($C_{10}H_{14}N_5O_7P$, AMP). STPP was chosen as the representative of AHP containing phosphoanhydride (P–O–P) bonds. EDTMP, PBTC and AMP were used as OP in this study. AMP is the natural OP containing phosphoester (P–O–C) bonds, EDTMP is the synthetic amino phosphonate (P–C–N), and PBTC is the synthetic nitrogen-free phosphonate (P–C). Potassium phosphate monobasic (KH_2PO_4, Ortho-P) was chosen for RP. The above reagents were all purchased from Shanghai Macklin Biochemical Co., Ltd (Shanghai, China), see Appendix A Table S1 for details. Besides, ascorbic acid, ammonium molybdate, antimony potassium tartrate, and sulfuric acid were all purchased from Sinopharm Chemical Reagent Co., Ltd. (Shanghai, China) and were used for the measurement of P. All chemicals used in this study were of analytical grade.

Construction waste CAAC was used as an adsorbent in the experiments and was crushed to the required sizes. The

CAAC used in lab-scale adsorption experiments was dried and ground to obtain uniform particle sizes (0.85–2.00 mm). The particle size of the CAAC used in the mesocosm study was about 2–3 cm.

1.2. Lab-scale study experimental procedure

1.2.1. Adsorption kinetics

The kinetic experiments were performed on four model NRP compounds (STPP, EDTMP, PBTC and AMP) and ortho-P. Accurately 3.0 g CAAC with a particle size of 0.85–2.00 mm was placed into a series of 250 mL conical flasks containing 150 mL P solutions, and the initial TP concentration was 10 mg/L. Two drops of toluene were also added to inhibit microbial activity. The conical flasks were shaken in a thermostatic oscillator of 180 r/min at 25°C for different time intervals, varying within 36 hr (0, 0.02, 0.1, 0.15, 0.25, 0.5, 1, 2, 4, 8, 16, 24 and 36 hr). Approximately 10 mL of supernatant was filtered through 0.22 μm polypropylene syringe filters and then the residual concentration of TP and soluble reactive phosphorus (SRP) was determined. Immediately after each sample, the pH of the remaining solution in the conical flasks was monitored using a portable pH meter (PHSJ-6L, INESA™ Analytical Instrument Co., Ltd., Shanghai, China). In addition, the effect of pH on NRP hydrolysis was investigated by a similar procedure using a 10 mg/L P solution (without the addition of CAAC) while maintaining pH at different values in the range of 3–9. Individual trials were analyzed for reaction rate by pseudo-first, pseudo-second, Intra-particle diffusion model and Elovich model based on the concentration of P remaining in the solution. The relevant equations are as follows:

The pseudo-first kinetic

$$\frac{dQ_t}{dt} = k_1(Q_e - Q_t) \tag{1}$$

where Q_t (mg/g) is the adsorbed amount at time t; Q_e (mg/g) is the adsorbed amount at equilibrium; k_1 (g/(mg·hr)) is the rate constant of pseudo-first-order adsorption.

The pseudo-second kinetic

$$\frac{dQ_t}{dt} = k_2(Q_e - Q_t)^2 \tag{2}$$

where k_2 (g/(mg·hr)) is the rate constant of pseudo-second-order adsorption.

Intra-particle diffusion model

$$Q_t = k_3 t^{0.5} + C \tag{3}$$

where k_3 (mg/(g·hr$^{0.5}$)) is the intraparticle diffusion rate constant; C is the intercept and reflects the thickness of the boundary layer.

Elovich model

$$Q_t = \frac{\ln a_e b_e}{b_e} + \frac{1}{b_e}\ln t \tag{4}$$

where the parameter a_e (mg/(g·hr)) is the initial adsorption rate, and b_e (g/mg) is related to extent of surface coverage and activation energy for chemisorptions.

1.2.2. Adsorption isotherms

The isotherm experiments were performed on four model NRP compounds (STPP, EDTMP, PBTC and AMP) and ortho-P. Accurately 3.0 g CAAC with a particle size of 0.85–2.00 mm was placed into 250 mL conical flasks containing 150 mL varying initial concentrations of P solutions. The initial concentrations of P solution were 0.1, 0.2, 0.4, 0.8, 1.5, 3.0, 5.0, 7.5, 10.0 mg/L, respectively. Two drops of toluene were added to restrict microbial activity The adsorption process lasted for 36 hr at 25°C in a thermostatic oscillator (ZHWY-2102, Jintan Jingda Instrument, China) with a speed of 180 r/min. After appropriate contact time, 10 mL of supernatant was filtered through 0.22 μm polypropylene syringe filters and then the residual concentration of TP and SRP was determined.

The equilibrium adsorption amounts of the P species were calculated using Eq. (5):

$$Q_e = (C_0 - C_e) \times V/M \tag{5}$$

where Q_e (mg/g) is the equilibrium adsorption capacity; C_0 (mg/L) and C_e (mg/L) are the initial and equilibrium concentrations of TP, respectively; V (L) is the total volume of the initial P solution; M (g) is the adsorbent mass.

The NRP adsorption performance of CAAC was evaluated in term of the partition coefficient (K_d, L/kg), which is simply a mass-weighted partition coefficient between solid phase and liquid supernatant phase as Eq. (6):

$$K_d = Q_e/C_e \tag{6}$$

The adsorption isotherms were investigated by the Langmuir model

$$1/Q_e = 1/K_l C_e Q_{max} + 1/Q_{max} \tag{7}$$

where K_l (L/mg) is the Langmuir adsorption rate constant; Q_{max} (mg/g) is the maximum saturated adsorption capacity; and the Freundlich model

$$\ln Q_e = \ln K_f + (1/n)\ln C_e \tag{8}$$

where K_f (mg/g) is the Freundlich adsorption rate constant; n is a heterogeneity parameter.

1.2.3. Desorption studies

The P desorption experiments were performed in conical flasks after the kinetic adsorption experiments. When the supernatant solution was removed, the CAAC was washed with 95% alcohol to remove the residual P solution, and 150 mL of 0.01 mol/L KCl solution was added to each conical flask. The subsequent operation was the same as the sorption kinetics experiments, except that the sampling intervals were changed to 0.5, 1, 2, 4, 8, 16, and 24 hr. Desorption efficiency (%) was defined as the ratio of the amount of P desorbed into the elution medium to the total amount of P adsorbed on the adsorbent.

1.3. Mesocosm study

To evaluate the adsorption and removal capacity of NRP species on CAAC after the scaling up of the reactors, a batch-loaded mesocosm experiment was conducted in a greenhouse

Table 1 – Initial concentrations of simulated water were measured at day 0.

	High concentration	Low concentration
Total phosphorus (mg/L)	2.76 ± 0.12	1.09 ± 0.14
Soluble reactive phosphorus (mg/L)	1.60 ± 0.15	0.44 ± 0.10
Non-reactive phosphorus (mg/L)	0.67 ± 0.06	0.27 ± 0.04
Particulate phosphorus (mg/L)	0.49 ± 0.15	0.37 ± 0.09
pH	7.74 ± 0.06	7.70 ± 0.12

at the Taihu Lake Water Research Center of Wuxi, Southeast University (31.48″ N, 120.37″ E). Four floating treatment wetlands (FTWs) were constructed using polypropylene board with dimensions of 120 cm in length, 30 cm in width, and 70 cm in height. The effective water depth of the reactor was 50 cm, and the total volume was 180 L. The 7 cm thick high-density polyethylene floating rafts with hanging baskets were used as the floating beds. The CAAC with a diameter of 2–3 cm was placed in the hanging basket, and the filling height was 9 cm (mass 3500 g and bulk density 450 g/L in each reactor). The simulated water was prepared by adding KH_2PO_4 and one of these NRP species to tap water. The system was operated in batch mode with two consecutive 7-day batches, and water sampling and analysis were performed on day 0 (initial), 1, 3, 5, and 7 of each batch. Water samples were immediately transported to the laboratory and then analyzed for water quality indicators within 3 hr. The two batches consist of a high concentration treatment followed by a low concentration treatment, and concentrations of simulated water measured at the beginning of each batch are shown in Table 1.

1.4. *Analysis and characterization*

The concentrations of TP, total dissolved phosphorus (TDP), and SRP in the system were measured in all experiments. Water samples for SRP and TDP were filtered through a 0.22 μm membrane filter (Millipore HAWP01300, USA). Samples for TDP and TP were digested by the persulfate digestion method. P samples were analyzed according to the ascorbic acid–molybdenum blue method (APHA, 2005) using a UV–VIS spectrophotometer (BlueStar–A proportional double-beam UV–VIS spectrophotometer, Labtech instruments co., LTD., China). All measurements of each sample were determined in triplicates. Furthermore, elemental compositions of CAAC were analyzed with X-ray fluorescence (XRF) spectrometry (Thermo Fisher Scientific, Waltham, USA). Scanning electron microscope (SEM) (ZEISS GeminiSEM 300, Germany) was used to characterize the morphology of the CAAC. BET surface areas were measured with a Micromeritics TriStar II 3020 physisorption analyzer.

The concentrations (C, mg/L) of soluble non-reactive phosphorus (SNRP) and particulate phosphorus (PP) were calculated according to the following equation:

$$C_{SNRP} = C_{TDP} - C_{SRP} \quad (9)$$

$$C_{PP} = C_{TP} - C_{TDP} \quad (10)$$

2. Results and discussion

2.1. *Physical and chemical properties of CAAC*

The CAAC is gray and the particle size is 0.85–2.00 mm (Appendix A Fig. S1a) and 2–3 cm (Appendix A Fig. S1b) for lab-scale adsorption experiments and mesocosm study, respectively. SEM analysis indicates the surface of CAAC is rough, porous and irregular, and widely distributed sheet-like structures interlace and support each other (Appendix A Fig. S1c, S1d), suggesting well-developed internal pores and a large specific surface area (BET surface area: 27.85 m^2/g). Furthermore, about 90% of the chemical composition of CAAC is CaO (32.1%), Al_2O_3 (19.5%) and SiO_2 (38.4%), and the active components, such as Ca^{2+}, Al^{3+} and Fe^{3+}, can be adsorption sites for P. The very interesting issue is the stability of CAAC in water. In this study, CAAC continuously dissolved in water and Ca was leached out to a concentration of about 30 mg/L (the leaching concentrations of Al and Fe less than 10 mg/L), also causing pH to rise to about 9.

2.2. *Adsorption kinetics*

Four typical kinetic models were used to simulate the adsorption kinetics of ortho-P and NRP on CAAC to identify the kinetic mechanism of the adsorption process. As the plots of adsorption kinetic curves shown in Fig. 1, the rapid adsorption of P occurred in the first 1 hr, and 90% of the maximum adsorption capacity (Q_{max}) could be achieved within 16 hr. This was similar to the adsorption process of phosphate on calcium-based substrate reported in previous studies (Markou et al., 2016). Comparing the kinetic parameters (Appendix A Table S2), it clearly revealed that the pseudo-second-order kinetic model presented good compliance with the obtained results for ortho-P, STPP, EDTMP and PBTC, suggesting that the rate-limiting step might be chemisorption. The pseudo-second-order model has been found to fit the sorption data in most of the studies, including the ortho-P adsorption on natural minerals, modified minerals and solid waste (Loganathan et al., 2014). Compared with ortho-P and other NRP, the correlation between AMP and the four kinetic models was lower. However, Elovich model still got relatively more fitness with a correlation coefficient (R^2) of 0.806. The Elovich equation is a semi-empirical rate model and assumes that the actual solid surfaces are energetically heterogeneous and the adsorption rate is related to the activation energy required for P adsorption (Collins et al., 2016). Previous studies have shown that this equation was suitable for describing phosphate ad-

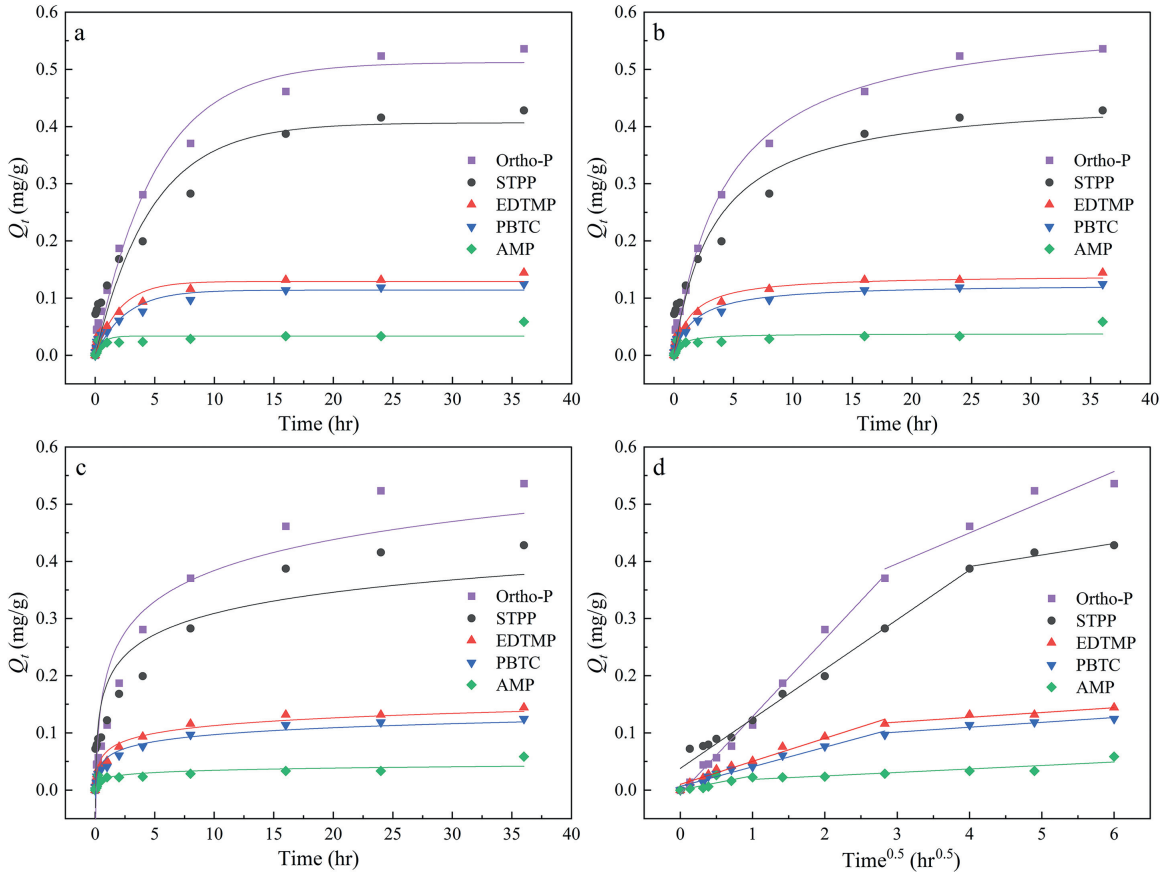

Fig. 1 – Kinetic models of P adsorption on CAAC ((a): the pseudo-first-order model, (b): the pseudo-second-order model, (c): the Elovich model, (d): the intraparticle diffusion model).

sorption kinetics on soil and sediment (Mezenner and Bensmaili, 2009). Although the equation does not propose any specific adsorbent-sorbent mechanism, it has been generally accepted that it can be used to describe chemisorption processes (Zhang and Stanforth, 2005). According to the intraparticle diffusion model, the multilinearity of P adsorption may be associated with the multi-step adsorption process (Pan et al., 2017). The early stage of the adsorption process was a linear region with greater slope values, implying the fast adsorption of P onto CAAC through boundary layer diffusion or macroporous diffusion at this stage. The slope values decreased at the later stage of the adsorption process, suggesting that the P adsorption was mainly attributed to the intraparticle diffusion or micropore diffusion, and the diffusion resistance increased, thus reducing the adsorption rate (Lopez et al., 2019). The k value (k_{intra1} and k_{intra2}) of ortho-P was higher than that of STPP and much larger than that of OP, indicating the faster adsorption rate of RP than NRP. The molecular size of P species may greatly affect the diffusion and adsorption rate given the same pore size (Wang et al., 2018).

The theoretical adsorption capacity at equilibrium (Q_e) calculated from the pseudo-second-order model was close to the kinetics experimental results, and the difference was less than 10.5%. The adsorption capacity of CAAC for different P species was in the order of ortho-P > STPP > EDTMP > PBTC > AMP. It was known from XRF data that there is abundant CaO in the CAAC, and calcium has a very strong positive effect on P adsorption (Nowack, 2003). The removal of ortho-P is assumed to be largely due to surface precipitation of calcium phosphate compounds or chemisorption. Conventionally, calcium phosphate precipitation in wastewaters can be achieved at increased pH (> 9) and/or increased concentration of calcium ions (Diamadopoulos, 1984). According to the variation of pH during the adsorption process in this study (Fig. 2b), ortho-P removal may be dominated by adsorption. The removal of STPP may depend on the reaction of Ca^{2+} released by CAAC with STPP to form amorphous Ca-STPP precipitate, or adsorption on substrate surface via relatively weak van der Waal's interactions (Zhou et al., 2011). The adsorption of the three OP (AMP, EDTMP, and PBTC) on CAAC was much weaker than that of ortho-P and STPP, which is consistent with the conclusion of Huang and Zhang (2011). It is noteworthy that the adsorption of OP compounds is compound specific. CAAC had the lowest adsorption capacity for AMP, with only 11.0% AMP removed at the end of the kinetic experiment. In contrast, the adsorption capacity of EDTMP on CAAC was larger and similar to PBTC. Adsorption of phosphonates depended on surface polarity (Nowack, 2003). Ca^{2+} on the surface of CAAC made the surface polarity more positive, reducing the charge repulsion to the phosphonate. Chemical interactions took place at the solid/water interface by the formation of ternary surface-phosphonate-Ca complexes (Liu et al., 2000). The adsorption

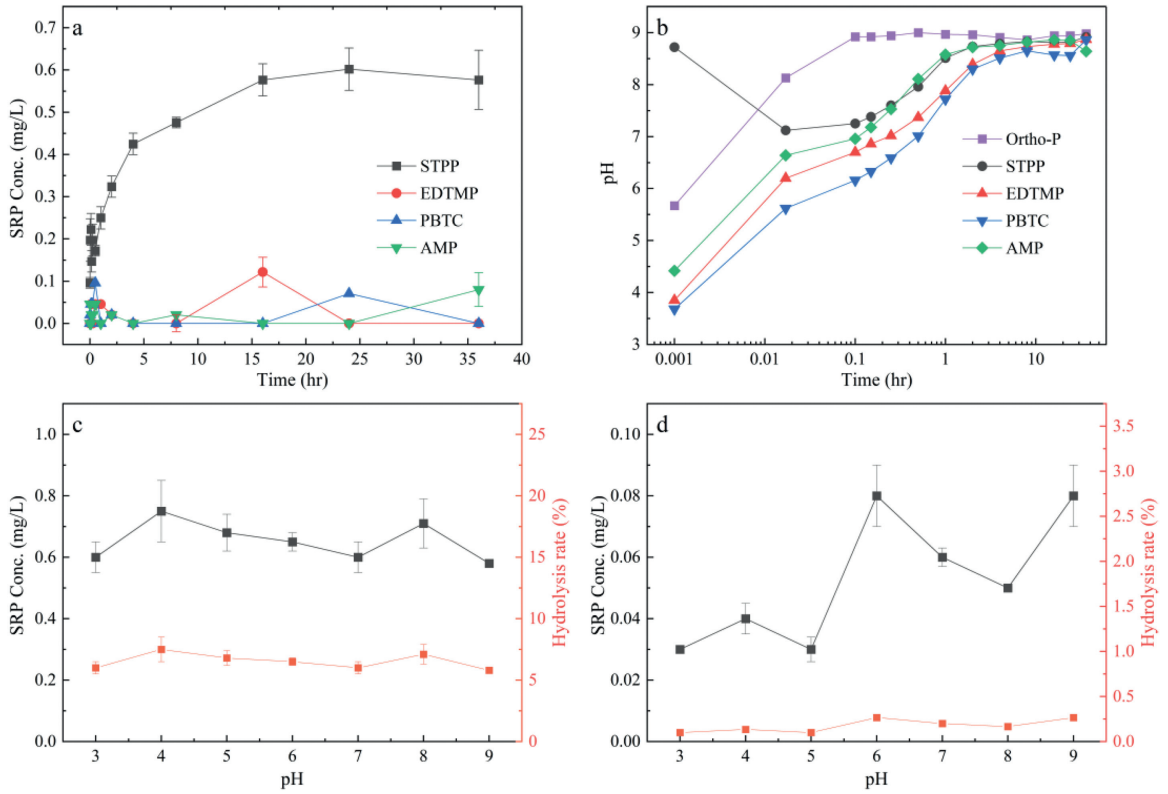

Fig. 2 – Variation of (a) SRP concentrations in different NRP systems and (b) pH value during adsorption kinetics experiment. Effect of pH on hydrolysis of (c) STPP and (d) OP.

capacity of PBTC on CAAC was weaker than that of EDTMP, which may be due to the fact that EDTMP with four phosphonate groups has a larger complex formation constant with bivalent metal ions than PBTC with one phosphonate group (Knepper, 2003), that is, EDTMP binds better with Ca^{2+}.

Hydrolysis of NRP to ortho-P in an aqueous solution may affect the removal of NRP by CAAC. The newly released ortho-P from added NRP may also participate in the sorption reaction with CAAC, and there may be adsorption competition between RP and NRP on the surface sites of CAAC (Huang and Zhang, 2011). As shown in Fig. 2a and b, only the hydrolysis of STPP was significant during the kinetics experiment. Due to the hydrolysis of STPP, the pH value decreased rapidly in the first 1 min of the experiment, and finally about 0.58 mg/L ortho-P was observed with a hydrolysis rate of 6.1%. Certainly, the hydrolysis of STPP was still very limited compared to the reduction of total STPP (92.3%). OP has high hydrolysis stability and is hydrolyzed only very slowly (Knepper, 2003). Among them (Fig. 3), EDTMP had a slightly higher hydrolysis rate, with the detected maximum hydrolysis rate of 1.3%. This result may be explained by the fact that the N-containing phosphonate EDTMP (P–C–N configuration) is more susceptible to light-independent hydrolysis than the N-free phosphonate PBTC (P–C configuration) (Schowanek and Verstraete, 1991). In addition, one experiment (without CAAC) performed at 25°C within the initial pH range of 3–9 showed that the hydrolysis rates of STPP and OP were 5.8%–7.5% and 0.1%–0.3%, respectively, indicating that pH had no significant effect on the NRP hydrolysis (Fig. 2c and d). It is worth noting that metallic cations such as Ca^{2+} and Mg^{2+} in aqueous solutions can provide additional NRP conversion to free ortho-P at a rate of approximately 1% per day (Nowack, 2003), which may explain the slightly higher OP hydrolysis rate (0.8%–1.3%) in this study.

2.2. *Adsorption isotherms*

The adsorption isotherm curves of different P species at 25°C were presented in Fig. 4. The classical Langmuir and Freundlich models were selected to evaluate the P adsorption capacity. Based on the correlation coefficient (Appendix A Table S3), it can be seen that both the models fit the data well within the given P concentration range. According to Freundlich model, the heterogeneity parameter n was in the range of 1–10, indicating favorable adsorption of P species on CAAC (Jellali et al., 2011). The theoretical Q_{max} of ortho-P on CAAC determined from the Langmuir isotherm was 1.45 mg/g, which was higher than other mineral and waste adsorbents such as concrete (0.1 mg/g), dolomite (0.17 mg/g), Limestone (0.3 mg/g) and apatite (1.09 mg/g) (Bellier et al., 2006; Prochaska and Zouboulis, 2006; Tao et al., 2020). The Q_{max} of CAAC for OP ranged between 0.18 and 0.25 mg/g. Some studies have shown that natural materials and minerals were also very potent adsorbents for NRP (Table 2). Vagi et al. (2010) revealed that the Q_{max} of OP on soil was less than 0.03 mg/g. Although the Ca-rich materials had a significant ability for P removal, Kumar et al. (2010) found that the adsorption of phosphonates on mussel shells was poor, with the Q_{max} less than 0.11 mg/g, and this could be the result of the low ac-

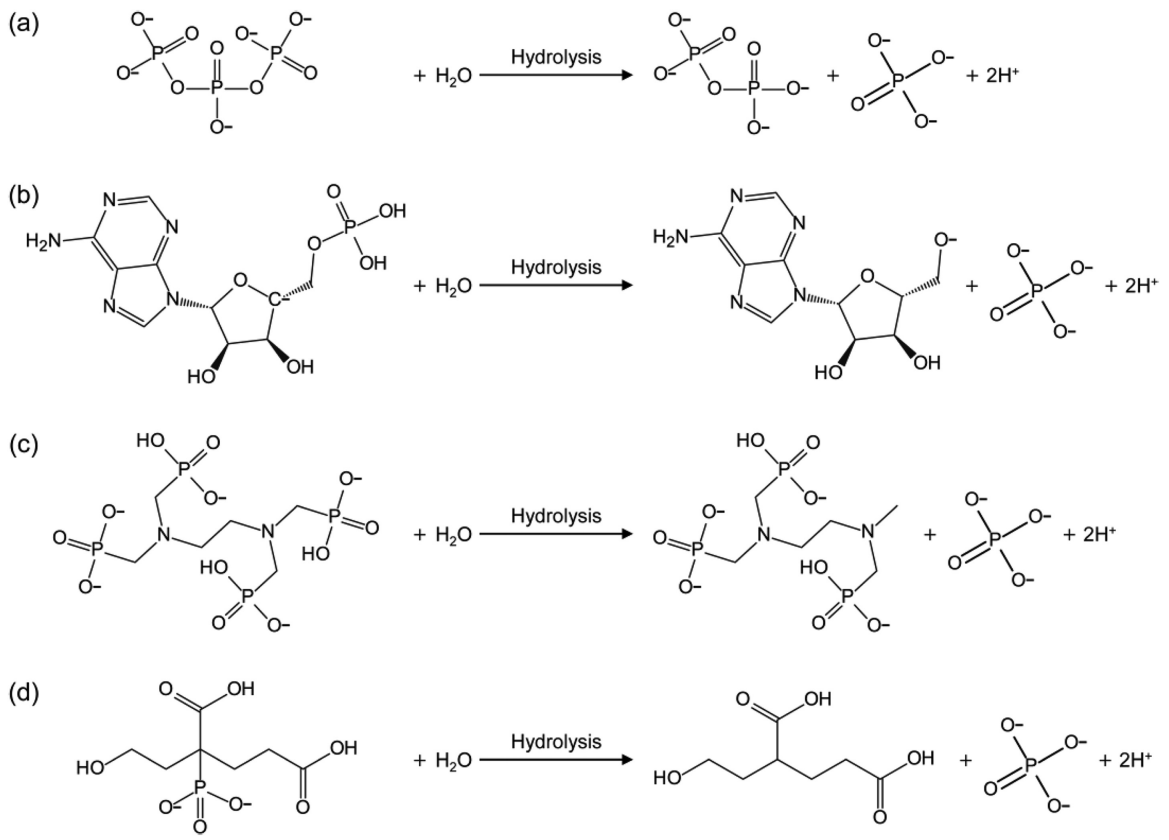

Fig. 3 – Hydrolysis of NRP. The reactions illustrate hydrolysis of the phosphoanhydride (P–O–P) bonds in (a) TPP and phosphoester (P–O–C) in (b) AMP, and hydrolysis of the P–C bonds in (c) EDTMP and (d) PBTC.

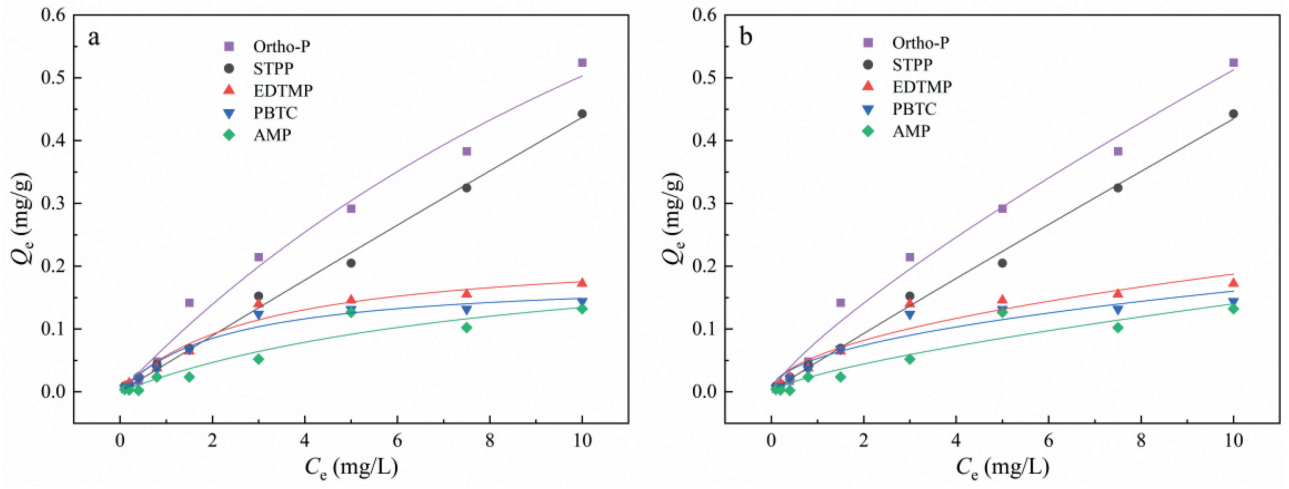

Fig. 4 – The isotherm plots of P adsorption on CAAC (a) Langmuir, (b) Freundlich.

tivity of calcium in the form of carbonate in mussel shells. Huang and Zhang (2011) also reached a similar conclusion that the adsorption of OP on carbonate sediments was much lower than that of phosphates. Moreover, iron and aluminum oxides or hydroxides, layered double hydroxides and high porous metal oxides/polymer composites generally have the highest P adsorption capacities compared with cheaper and more readily available adsorbents such as by-products, waste or natural materials. Surface modification of adsorbents by heat or acid treatment and grafting of metals or organic functional groups can further improve the adsorption capacity (Loganathan et al., 2014). Chen et al. (2017) showed that the adsorption capacity of granular ferric hydroxide for phosphonates was more than 1.12 mg/g, but the adsorbent could not be effectively regenerated and was not cost-effective. The covalent organic framework synthesized via the irreversible enol-

Table 2 – Comparison of NRP adsorption with previous adsorbents.

Adsorbent	P species	Bond types	C_0 (mg/L)	Q_{max} (mg/g)	Ref.
Covalent Organic Frameworks	Triphenyl phosphate (TPhP)	Phosphoester (P–O–C)	1.9	86.1–387.2	(Wang et al., 2018)
Granular ferric hydroxide	Nitrilotri (methylphosphonic) acid (NTMP)	P–C	0.6–9.0	$1.12–1.01 \times 10^4$	(Chen et al., 2017)
Magnetic multi-walled carbon nanotubes	Profenofos	Phosphoester (P–O–C)	2	3.89	(Liu et al., 2018)
Mussel shells	potassium phosphonate	P–C	20	0.11	(Kumar et al., 2010)
Soil	O,O-dimethyl S-methylcarbamoylmethyl phosphorodithioate	Phosphoester (P–O–C), P–S	20	0.01–0.03	(Vagi et al., 2010)
Soil	O,O-dimethyl O-4-methylthio-m-tolyl phosphorothioate	Phosphoester (P–O–C), P–S	20	0.09–0.17	(Vagi et al., 2010)

Table 3 – Partition coefficients of different phosphorus species adsorption on CAAC at different initial concentrations.

C_0 (mg/L)	K_d (L/kg)				
	Ortho-P	STPP	EDTMP	PBTC	AMP
0.1	773.75	-	-	-	61.11
0.2	1250.00	1811.29	2028.07	1114.86	27.78
0.4	1369.21	1701.22	1057.40	967.00	9.21
0.8	1684.21	1492.45	854.00	455.42	52.46
1.5	2400.13	891.86	313.21	309.34	19.88
3.0	2233.96	667.18	126.28	168.32	24.15
5.0	1988.36	527.41	56.54	77.64	46.09
7.5	1184.08	602.40	32.40	44.69	27.24
10.0	1070.71	593.25	21.23	18.02	6.80

toketo tautomerization between 1,3,5-triformylphloroglucinol and benzidine exhibited an excellent adsorption affinity for OP, with the Q_{max} up to 387.2 mg/g (Wang et al., 2018). However, the activation and surface modification of adsorbents increase the cost of adsorbents, and a cost-benefit analysis is necessary to determine their economic feasibility.

The partition coefficients of different P species adsorption on CAAC at different initial concentrations are shown in Table 3. The K_d of Ortho-P on CAAC increased first and then decreased with the increase of initial P concentration, while the K_d of STPP, EDTMP and PBTC on CAAC decreased gradually. The K_d of AMP on CAAC was relatively small and showed no obvious trend. It could be speculated that the lower the concentration of such NRP as STPP, EDTMP and PBTC, the stronger the binding with CAAC (Chouyyok et al., 2010).

2.3. *Desorption studies*

P species are closely related to the desorption characteristics and indicate the P mobility and bioavailability. The desorption curves (Fig. 5) show that almost no ortho-P was desorbed and its maximum desorption efficiency was lower than 0.02%, which was likely caused by the formation of inner-sphere complexes or diffusion into the interior pores and channels of the substrates (Loganathan et al., 2014), and the chemisorption between ortho-P and CAAC resulted in extremely low desorption potential. This is consistent with the conclusion of Lopez et al. (2019). Considering the difference in P adsorption and desorption rates within the time scale of the desorption experiment (24 hr), the adsorption of ortho-P could be reversible if sufficient time and low enough P concentration were given (Lai and Lam, 2009).

During the desorption experiment, NRP desorption occurred rapidly and reached equilibrium in about 4 hr. The desorption capacity of STPP and AMP decreased after reaching the peak value, which might be because the desorbed NRP was readsorbed or hydrolyzed into SRP. Among the four NRP model compounds, STPP had the highest desorption capacity with 0.06 mg/g (NRP accounted for 50.5%), but its desorption efficiency was the lowest, and only 14.8% of the previously adsorbed STPP was released back into the solution. The desorption of OP was greater than that of phosphates, and the total maximum desorption efficiencies of EDTMP, PBTC and AMP were 20.46%, 18.33% and 29.50%, respectively. This suggests that Ca tended to form complexes with OP, which were much less stable than those formed with phosphates. However, most NRP was still irreversibly adsorbed. Morillo et al. (1997) observed that almost 40% of glyphosate previously adsorbed by montmorillonite desorbed, indicating that the adsorption of OP onto the clay mineral was not completely reversible. Chen et al. (2017) reported that only 40%–50% of the adsorbed phosphonate adsorbed by granular ferric hydroxide were released within 24 hr even in 1.0 mol/L NaOH solutions. This desorption behavior also indicates that the adsorption mech-

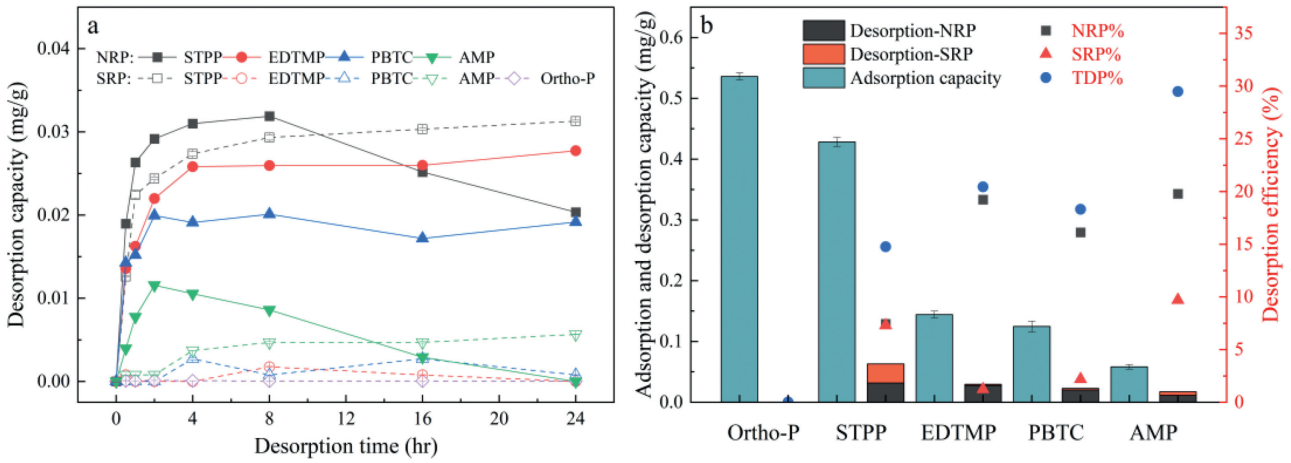

Fig. 5 – (a) Phosphorus desorption of adsorbed CAAC in KCl solution and (b) the corresponding desorption efficiency. The solid line indicates the amount of NRP desorbed (mg/g), and the dotted line indicates the amount of SRP desorbed (mg/g).

anism involved inner-sphere complexation. Furthermore, the desorption process seemed to follow the same two-stage pattern as diffusion into the pores or solids during adsorption, until equilibrium was reached. The desorption of STPP, EDTMP and PBTC showed a slow stage, suggesting that intraparticle diffusion was the rate-controlled step for their adsorption (Zhang and Stanforth, 2005). When desorption processes take place, a small portion of the absorbed OP could be replaced by water or anion (e.g. OH^- and Cl^-) on the substrate surface, as Morillo et al. (1997) suggested which occurred in the case of glyphosate adsorption by the clay mineral montmorillonite or hematite. This part of NRP desorbed in KCL solution may be bounded with CAAC through ion exchange or outer-sphere complexation (Markou et al., 2016).

2.4. *Mesocosm study*

A mesocosm study was conducted to investigate the short-term dynamics and performance of CAAC removing NRP at two concentration levels (Fig. 6). In high P conditions, the concentration of SNRP and PP showed a decreasing trend. With an hydraulic retention time of 7 days, the removal efficiencies of STPP, EDTMP, PBTC and AMP were 70.5%, 33.9%, 63.2% and 89.3%, respectively. In low P conditions, SNRP and PP concentrations showed a decreasing trend, while an increase in SRP concentration was observed during the experiment. Different from the results of laboratory adsorption experiments, AMP achieved the highest removal efficiency. AMP, as a natural OP from plants, animals, or microbial cellular materials (Venkiteshwaran et al., 2018), is involved in cellular energy transfer and easily used by various microorganisms (Baldwin, 2013). AMP can be utilized even in the presence of ortho-P which is the preferred P substrate for bacteria and algae. This finding is consistent with that of Lovdal et al. (2007). Similarly, the availability of ortho-P did not limit the removal of the other three NRP. The removal of PBTC in the mesocosm experiment was better than that in the adsorption experiment. It was found that PBTC can be degraded slowly in a natural environment, and the PBTC-utilizing microorganisms could not be assigned to a specific bacterial family (Rott et al., 2018). Raschke et al. (1994) reported that PBTC was rapidly degraded even in the presence of 0.01 mm (0.95 mg/L) ortho-P. In contrast, other studies have found that 95% of PBTC was retained in the sewage sludge and would not be effectively degraded (Knepper, 2003). Approximately 27.9%–33.9% EDTMP conversion was obtained after 7 days at two concentration levels, which was superior to previous studies that showed an abiotic conversion rate of about 15% for the N-containing phosphonates after 7 days (Schowanek and Verstraete, 1991). Therefore, when evaluating the adsorption capacity of CAAC for NRP in natural systems, biodegradation processes may become essential for the conversion and removal of NRP in addition to the pathway of adsorption, precipitation, and natural hydrolysis. Moreover, an increase in SRP concentration was observed during the experiment, especially in low P conditions. Considering that ortho-P absorbed by CAAC was difficult to be released, the increase of SRP concentration was most likely due to the hydrolysis of NRP. In low P conditions, the hydrolysis of STPP ultimately resulted in a negative TP removal efficiency, which means that the NRP adsorbed by CAAC under the high P concentration of the previous batch may be released and hydrolyzed in the following low P condition. CAAC alone was not sufficient to maintain stable treatment efficiency in the face of inflow P load fluctuations.

2.5. *Cost-benefit analysis*

CAAC is a highly available building material used worldwide and it accounts for the majority of construction wastes, which are large in quantity and difficult to dispose and recycle (Bao et al., 2020). It can be assumed that the application of waste materials is free and it can even reduce disposal costs and create additional environmental benefits. CAAC is simple in composition and stable in quality, which would not produce excessively high pH in the effluents and the risk of releasing heavy metals and other hazardous substances could be eliminated (Shen et al., 2022). Several studies dealt with the pretreatment of adsorbents with Zr, La, Fe, or other reagents to increase adsorption capacity, however, these surface-modified adsorbents exhibited many

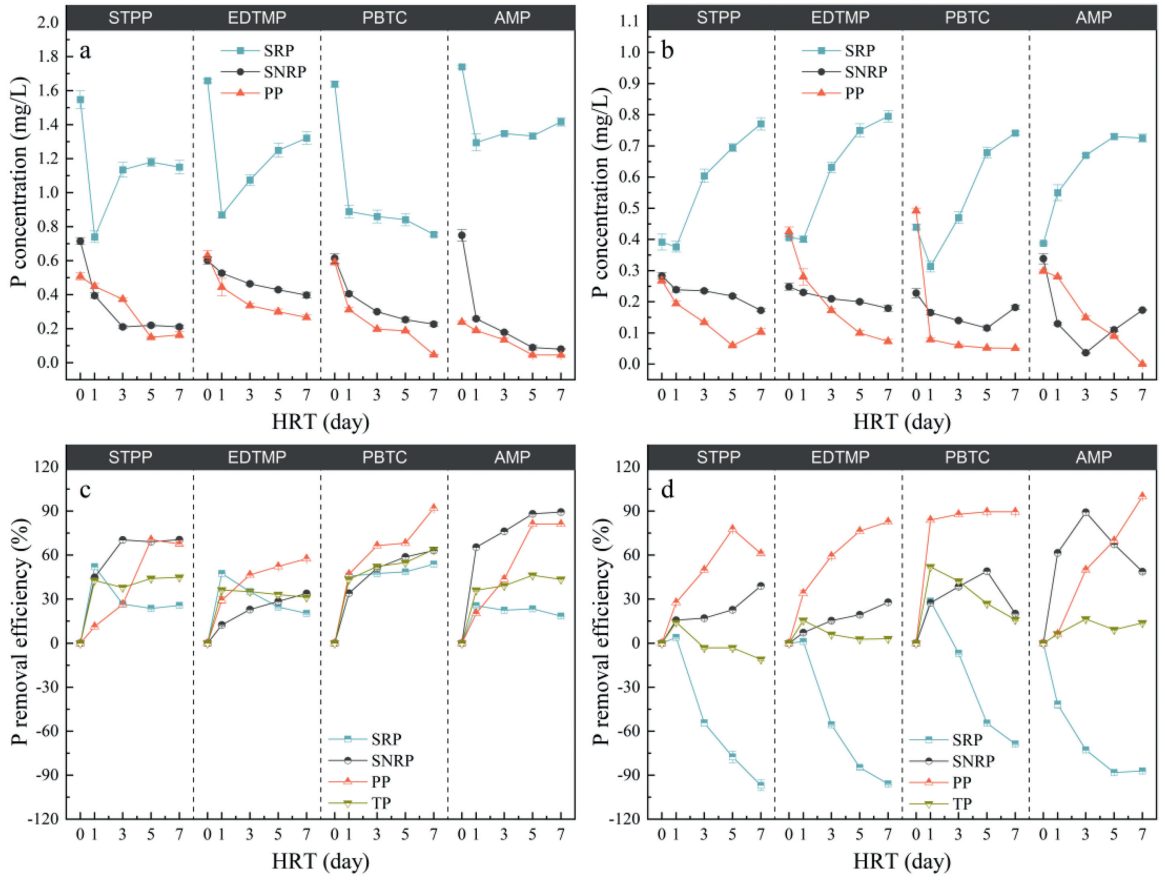

Fig. 6 – Changes in concentrations of different forms of P at (a) low and (b) high P concentrations and corresponding removal efficiency at (c) low and (d) high P concentrations in the mesocosm study.

disadvantages in cost-effectiveness and environmental impact (Kumwimba et al., 2018). A major disadvantage of by-products such as alum sludge and steel slag is their unstable quality due to variable conditions of the production process (Kasprzyk et al., 2021). The high pH (> 9) of many alkaline substrates could also be a limitation in their application (Blanco et al., 2016). For sustainability of a circular economy, CAAC can be exploited as a P-rich material for agricultural purposes after the adsorption capacity is exhausted (Castellar et al., 2019). The P recovery potential and further reuse (fertilizer and industrial use) of CAAC after NRP adsorption requires further investigation.

3. Conclusions

This study investigated the potential and mechanism of construction waste CAAC removing different NRP species. Results of kinetic experiments showed that CAAC adsorbed about 90% of NRP within the first 16 h, and the removal of NRP was a chemisorption process and also involved a two-step pore diffusion process. It was evident that RP was liberated through NRP conversion, and the hydrolysis rates of STPP and three kinds of OP (EDTMP, PBTC, and AMP) were 5.8%–7.5% and 0.8%–1.3%, respectively. NRP hydrolysis into RP in an aqueous solution may affect the removal of NRP by CAAC. The maximum theoretical adsorption capacity of CAAC for STPP calculated from the Langmuir isotherm was 1.24 mg/g, followed by OP, which ranged between 0.18 and 0.25 mg/g. During the desorption experiment, almost no ortho-P was desorbed, and different NRP species showed varying degrees of desorption, with the maximum desorption efficiency less than 29.5%. This indicates that most NRP was irreversibly adsorbed on CAAC, and the adsorption mechanism involved inner-sphere complexation. Different from the lab-scale adsorption experiments, the results of the mesocosm study showed that the possible biodegradation was essential for the conversion and removal of NRP in addition to the adsorption of NRP by CAAC. The research performed proved the validity of CAAC for NRP removal and the potential advantages of CAAC in terms of costs and environmental impact. The long-term dynamics of adsorption and desorption of NRP by CAAC in practical applications should be an aim of further studies to better evaluate the potential of CAAC for NRP removal and the risk of eutrophication caused by NRP.

Declaration of Competing Interest

The authors declare that they have no known competing financial interests or personal relationships that could have appeared to influence the work reported in this paper.

Acknowledgment

This work was supported by the Major Science and Technology Program for Water Pollution Control and Treatment in China (No. 2017ZX07202004). The authors would like to thank the shiyanjia lab (www. shiyanjia.com) for the XRF test.

Appendix A Supplementary data

Supplementary material associated with this article can be found, in the online version, at doi:10.1016/j.jes.2022.07.006.

REFERENCES

APHA, 2005. Standard Methods for the Examination of Water and Wastewater. American Public Health Association, Washington, DC.

Baldwin, D.S., 2013. Organic phosphorus in the aquatic environment. Environ. Chem. 10, 439–454.

Bao, T., Yu, Z.M., Damtie, M.M., Wu, K., Jin, J., Zhang, Y., et al., 2020. Use of autoclaved aerated concrete particles for simultaneous removal of nitrogen and phosphorus as filter media from domestic wastewater. Environ. Technol. 41, 3032–3042.

Bellier, N., Chazarenc, F., Comeau, Y., 2006. Phosphorus removal from wastewater by mineral apatite. Water Res. 40, 2965–2971.

Blanco, I., Molle, P., Saenz de Miera, L.E., Ansola, G., 2016. Basic oxygen furnace steel slag aggregates for phosphorus treatment. Evaluation of its potential use as a substrate in constructed wetlands. Water Res. 89, 355–365.

Castellar, F., Chimenos, C., Bosch, R., Canal, J., Bosch, M., Rosell, J.R., et al., 2019. Crushed autoclaved aerated concrete (CAAC), a potential reactive filter medium for enhancing phosphorus removal in nature-based solutions—preliminary batch studies. Water 11 (7), 1442.

Chen, Y., Baygents, J.C., Farrell, J., 2017. Removing phosphonate antiscalants from membrane concentrate solutions using granular ferric hydroxide. J. Water Process Eng. 19, 18–25.

Chouyyok, W., Wiacek, R.J., Pattamakomsan, K., Sangvanich, T., Grudzien, R.M., Fryxell, G.E., et al., 2010. Phosphate removal by anion binding on functionalized nanoporous sorbents. Environ. Sci. Technol. 44, 3073–3078.

Collins, S.D., Shukla, S., Shrestha, N.K., 2016. Drainage ditches have sufficient adsorption capacity but inadequate residence time for phosphorus retention in the Everglades. Ecol. Eng. 92, 218–228.

Cordell, D., White, S., 2014. Life's Bottleneck: sustaining the world's phosphorus for a food secure future. Ann. Rev. Environ. Res. 39, 161–188.

Diamadopoulos, E., 1984. The precipitation of phosphorus from wastewater through pH variation in the presence and absence of coagulants. Water Res. 18, 1175–1179.

Diaz, R.J., Rosenberg, R., 2008. Spreading dead zones and consequences for marine ecosystems. Science 321, 926–929.

Dires, S., Birhanu, T., Ambelu, A., 2019. Use of broken brick to enhance the removal of nutrients in subsurface flow constructed wetlands receiving hospital wastewater. Water Sci. Technol. 79, 156–164.

Dodds, W.K., Bouska, W.W., Eitzmann, J.L., Pilger, T.J., Pitts, K.L., Riley, A.J., et al., 2009. Eutrophication of US freshwaters: analysis of potential economic damages. Environ. Sci. Technol. 43, 12–19.

Gray, H.E., Powell, T., Choi, S., Smith, D.S., Parker, W.J., 2020. Organic phosphorus removal using an integrated advanced oxidation-ultrafiltration process. Water Res. 182, 115968.

Huang, X.L., Zhang, J.Z., 2011. Phosphorus sorption on marine carbonate sediment: phosphonate as model organic compounds. Chemosphere 85, 1227–1232.

Jellali, S., Wahab, M.A., Ben Hassine, R., Hamzaoui, A.H., Bousselmi, L., 2011. Adsorption characteristics of phosphorus from aqueous solutions onto phosphate mine wastes. Chem. Eng. J. 169, 157–165.

Kasprzyk, M., Czerwionka, K., Gajewska, M., 2021. Waste materials assessment for phosphorus adsorption toward sustainable application in circular economy. Resour. Conserv. Recycl. 168.

Knepper, T., 2003. Synthetic chelating agents and compounds exhibiting complexing properties in the aquatic environment. TrAC Trends Anal. Chem. 22, 708–724.

Kumar, R.A., Velayudhan, K.T., Ramachandran, V., Bhai, R.S., Unnikrishnan, G., Vasu, K., 2010. Adsorption and removal kinetics of phosphonate from water using natural adsorbents. Water Environ. Res. 82, 62–68.

Kumwimba, M.N., Meng, F.G., Iseyemi, O., Moore, M.T., Bo, Z., Tao, W., et al., 2018. Removal of non-point source pollutants from domestic sewage and agricultural runoff by vegetated drainage ditches (VDDs): Design, mechanism, management strategies, and future directions. Sci. Total Environ. 639, 742–759.

Lai, D.Y.F., Lam, K.C., 2009. Phosphorus sorption by sediments in a subtropical constructed wetland receiving stormwater runoff. Ecol. Eng. 35, 735–743.

Lei, Y., Saakes, M., van der Weijden, R.D., Buisman, C.J.N., 2020. Electrochemically mediated calcium phosphate precipitation from phosphonates: implications on phosphorus recovery from non-orthophosphate. Water Res. 169, 115206.

Liu, G., Li, L., Huang, X., Zheng, S., Xu, X., Liu, Z., et al., 2018. Adsorption and removal of organophosphorus pesticides from environmental water and soil samples by using magnetic multi-walled carbon nanotubes @ organic framework ZIF-8. J. Mater. Sci. 53, 10772–10783.

Liu, Y., Gao, L., Yu, L., Guo, J., 2000. Adsorption of PBTCA on alumina surfaces and its influence on the fractal characteristics of sediments. J. Colloid Interface Sci. 227, 164–170.

Loganathan, P., Vigneswaran, S., Kandasamy, J., Bolan, N.S., 2014. Removal and recovery of phosphate from water using sorption. Crit. Rev. Environ. Sci. Technol. 44, 847–907.

Lopez, R., Antelo, J., Fiol, S., Macias-Garcia, F., 2019. Phosphate adsorption on an industrial residue and subsequent use as an amendment for phosphorous deficient soils. J. Clean. Prod. 230, 844–853.

Lovdal, T., Tanaka, T., Thingstad, T.F., 2007. Algal-bacterial competition for phosphorus from dissolved DNA, ATP, and orthophosphate in a mesocosm experiment. Limnol. Oceanogr. 52, 1407–1419.

Markou, G., Mitrogiannis, D., Muylaert, K., Celekli, A., Bozkurt, H., 2016. Biosorption and retention of orthophosphate onto $Ca(OH)_2$-pretreated biomass of *Phragmites* sp. J. Environ. Sci. 45, 49–59.

Mezenner, N.Y., Bensmaili, A., 2009. Kinetics and thermodynamic study of phosphate adsorption on iron hydroxide-eggshell waste. Chem. Eng. J. 147, 87–96.

Morillo, E., Undabeytia, T., Maqueda, C., 1997. Adsorption of glyphosate on the clay mineral montmorillonite: effect of Cu(II) in solution and adsorbed on the mineral. Environ. Sci. Technol. 31, 3588–3592.

Nowack, B., 2003. Environmental chemistry of phosphonates. Water Res. 37, 2533–2546.

Pan, M., Lin, X.M., Xie, J., Huang, X., 2017. Kinetic, equilibrium and thermodynamic studies for phosphate adsorption on aluminum hydroxide modified palygorskite nano-composites. RSC Adv. 7, 4492–4500.

Pramanik, B.K., Islam, M.A., Asif, M.B., Roychand, R., Pramanik, S.K., Shah, K.W., et al., 2020. Emerging investigator series: phosphorus recovery from municipal wastewater by adsorption on steelmaking slag preceding forward osmosis: an integrated process. Environ. Sci. Water Res. Technol. 6, 1559–1567.

Prochaska, C.A., Zouboulis, A.I., 2006. Removal of phosphates by pilot vertical-flow constructed wetlands using a mixture of sand and dolomite as substrate. Ecol. Eng. 26, 293–303.

Raschke, H., Rast, H.G., Roland, K., Sicius, H., Wischer, D., 1994. Utilization of 2-phosphonobutane-1,2,4-tricarboxylic acid as source of phosphorus by environmental bacterial isolates. Chemosphere 29, 81.

Rittmann, B.E., Mayer, B., Westerhoff, P., Edwards, M., 2011. Capturing the lost phosphorus. Chemosphere 84, 846–853.

Rott, E., Steinmetz, H., Metzger, J.W., 2018. Organophosphonates: a review on environmental relevance, biodegradability and removal in wastewater treatment plants. Sci. Total Environ. 615, 1176–1191.

Schowanek, D., Verstraete, W., 1991. Hydrolysis and free radial mediated degradation of phosphonates. J. Environ. Qual. 20, 769–776.

Shen, S., Geng, Z., Li, X., Lu, X., 2022. Evaluation of phosphorus removal in floating treatment wetlands: new insights in non-reactive phosphorus. Sci. Total Environ. 815, 152896.

Shen, S., Li, X., Cheng, F., Zha, X., Lu, X., 2020. Review: recent developments of substrates for nitrogen and phosphorus removal in CWs treating municipal wastewater. Environ. Sci. Pollut. Res. Int. 27, 29837–29855.

Shi, X., Fan, J., Zhang, J., Shen, Y., 2017. Enhanced phosphorus removal in intermittently aerated constructed wetlands filled with various construction wastes. Environ. Sci. Pollut. Res. Int. 24, 22524–22534.

Smil, V., 2002. Phosphorus: global transfers - causes and consequences of global environmental change. Annu. Rev. Energy Environ. 25, 53–88.

Tao, B., Li, W., Xie, L., Yu, J., He, F., 2020. Performance analysis of demolition waste bricks for phosphorus removal from stormwater runoff. Urban Water J. 17, 144–153.

Vagi, M.C., Petsas, A.S., Kostopoulou, M.N., Lekkas, T.D., 2010. Adsorption and desorption processes of the organophosphorus pesticides, dimethoate and fenthion, onto three Greek agricultural soils. Int. J. Environ. Anal. Chem. 90, 369–389.

Venkiteshwaran, K., McNamara, P.J., Mayer, B.K., 2018. Meta-analysis of non-reactive phosphorus in water, wastewater, and sludge, and strategies to convert it for enhanced phosphorus removal and recovery. Sci. Total Environ. 644, 661–674.

Wang, W., Deng, S., Ren, L., Li, D., Wang, W., Vakili, M., et al., 2018. Stable covalent organic frameworks as efficient adsorbents for high and selective removal of an Aryl-Organophosphorus flame retardant from water. ACS Appl. Mater. Interfaces 10, 30265–30272.

Yang, Y., Wang, Z.M., Liu, C., Guo, X.C., 2012. Enhanced P, N and C removal from domestic wastewater using constructed wetland employing construction solid waste (CSW) as main substrate. Water Sci. Technol. 66, 1022–1028.

Zhang, J., Stanforth, R., 2005. Slow adsorption reaction between arsenic species and goethite (alpha-FeOOH): diffusion or heterogeneous surface reaction control. Langmuir 21, 2895–2901.

Zhou, J., Xu, Z.P., Qiao, S., Liu, Q., Xu, Y., Qian, G., 2011. Enhanced removal of triphosphate by MgCaFe-Cl-LDH: synergism of precipitation with intercalation and surface uptake. J. Hazard. Mater. 189, 586–594.